J Math Chem (2008) 44:884–912
DOI 10.1007/s10910-007-9337-4

ORIGINAL PAPER

Unequivocal disentangling genuine from spurious information in time signals: clinical relevance in cancer diagnostics through magnetic resonance spectroscopy

Dževad Belkić · Karen Belkić

Received: 13 November 2007 / Accepted: 27 November 2007 / Published online: 9 February 2008

Abstract Pole-zero cancellation in the polynomial quotient of the fast Padé transform (FPT) is shown to clearly and unequivocally distinguish spurious resonances from the true metabolites, in the presence of random Gauss-distributed zero mean noise in a magnetic resonance (MR) spectrum. Thus, by applying the principle of Froissart doublets within the FPT, noise as typically encountered in clinically encoded MR-time signals, is completely separated from the genuine metabolic information. The basis for the unprecedented algorithmic success of the FPT for processing of MR signals is explained within the framework of quantum mechanics. The clear, direct and immediate importance of these findings is reviewed with respect to clinical oncology. Besides confirming the high resolution and stability of the FPT in general studies of MR total shape spectra, this superior resolution performance of the FPT has also been confirmed with respect to data directly derived from malignant and benign ovarian samples. Not only does the FPT markedly enhance resolution of MR spectra compared to the conventional Fourier analysis, but it also yields the unequivocal, exact parametric data needed to reconstruct the metabolite concentrations which characterize ovarian cancer and distinguish this from non-malignant lesions. These features of the FPT are deemed to be of critical benefit to ovarian cancer diagnostics via MRS, in particular for early detection, a goal which has thus far been elusive, but achievement of which would definitely confer a major survival advantage. It is anticipated that MRS via Padé processing will reduce the false positive rates of MR-based modalities and, moreover, will further improve the sensitivity of these methods. Once this is achieved,

Dž. Belkić (✉) · K. Belkić
Department of Oncology/Pathology, Karolinska Institute, P.O. Box 260, Stockholm 17176, Sweden
e-mail: Dzevad.Belkic@ki.se

K. Belkić
Institute for Prevention Research, University of Southern California Keck School of Medicine,
Los Angeles, CA 91803, USA
e-mail: Karen.Belkic@ki.se

and given that all MR-based diagnostic methods are free from ionizing radiation, new possibilities for cancer screening and early detection would emerge, especially for risk groups, e.g., the application of Padé-optimized MRS in younger women at high risk for breast and/or ovarian cancer.

Keywords Padé approximant · Fast Padé transform · Froissart doublets · Pole-zero cancellations · Magnetic resonance spectroscopy · Cancer diagnostics

Abbreviations

Ala	Alanine
AMARES	Advanced Method for Accurate Robust and Efficient Spectral fitting
au	Arbitrary units
Cho	Choline
C_{met}	Metabolite concentration
Cr	Creatine
Crn	Creatinine
FID	Free induction decay
FFT	Fast Fourier transform
FPT	Fast Padé transform
FWHM	Full width at half maximum
GABA	Gamma amino butyric acid
Glu	Glutamate
Gln	Glutamine
Glc	Glucose
HLSVD	Hankel-Lanczos Singular Value Decomposition
ICR-MS	Ion-cyclotron resonance mass spectroscopy
Iso	Isoleucine (Iso)
Lac	Lactate
LCModel	Linear Combination of Model in vitro Spectra
LP	Linear predictor
Lys	Lysine
Met	Methionine
MR	Magnetic resonance
MRI	Magnetic resonance imaging
MRS	Magnetic resonance spectroscopy
MRSI	Magnetic resonance spectroscopic imaging
NAA	N-acetyl aspartate
NAAG	N-acetyl aspartyl glutamate
PA	Padé approximant
ppm	Parts per million
PSA	Prostate specific antigen
SNR	Signal-to-noise ratio
SNS	Signal–noise separation
Thr	Threonine
Val	Valine
VARPRO	Variable Projection Method

1 Introduction

1.1 The need to go beyond conventional data analysis

Our overall goal is to improve cancer diagnostics on *a quantitative molecular basis* by retrieving key information that remains undetected with conventional data analysis, such as the fast Fourier transform (FFT) and post processing via fitting and/or peak integrations.

1.1.1 Paradigm shift

The undetected information can nevertheless be extracted by the novel and self-contained data analysis, via the fast Padé transform (FPT), which we have recently introduced and implemented into magnetic resonance spectroscopy (MRS) [1–12]. This was made possible by widening the horizons of signal processing through finding its natural framework in a larger and well-established theory—quantum physics [12]. By identifying the quantification problem in signal processing as quantum-mechanical spectral analysis, the key door was opened for using a highly-developed mathematical apparatus (eigenvalue problems, etc.) to successfully overcome the otherwise insurmountable difficulties of the FFT, fittings and the like [5,6,8]. It is through this direct connection of signal processing with quantum physics that a veritable *paradigm shift* has been established, and the stage set for the emergence of the powerful and versatile spectral analyzer—the FPT. From the standpoint of mathematical modelling, the FPT is capable of extracting the missing information from the analyzed time signals, because it has more degrees of freedom via the use of two polynomials in the form of their ratio P/Q rather than only one such polynomial encountered in the FFT. Mathematical modelling is indispensable in signal processing, since no encoded time signal can be interpreted directly in terms of the sought, clinically relevant information—the concentrations of metabolites from the tissue scanned by MRS.

1.1.2 Novel and advantageous data analysis

We have demonstrated that the FPT is the signal processing *method of choice* to achieve the above-stated goal. We have performed the "*proof of principle*" investigations establishing that the FPT meets the most stringent criteria imposed by clinical disciplines such as oncology for MRS and MR spectroscopic imaging (MRSI) [1–12].

The high resolution and stability of the FPT have been clearly confirmed in studies of total shape spectra [1–4,11], thereby overcoming one of the major hindrances to wider application of MRS and MRSI in clinical oncology.

However, as explained in detail in [13], total shape spectra do not provide the information needed to determine how many metabolites are actually present and in which concentrations. It is this information which is most vital for improving the diagnostic yield and accuracy of MRS and MRSI in oncology.

Most recently, using the FPT we have performed the benchmark studies in which this method was shown to provide *exact quantification* of MRS signals and thereby

metabolite concentrations are reliably and unequivocally obtained with an intrinsic and robust error analysis [5,7,8]. These studies are summarized briefly herein.

We have also demonstrated that the FPT unambiguously distinguishes genuine from spurious peaks in MR spectra. The number of spurious resonances is always several times larger than the number of genuine resonances. It is of utmost importance for trustworthy clinical applications that the genuine information is identified with certainty by confidently disentangling it from noise. As reviewed herein, via the powerful concept of Froissart doublets (pole-zero cancellations), the FPT is shown to achieve this task [6]. The *clinical significance* of this capability of the FPT is best appreciated by recalling that measured MRS time signals are always corrupted with noise and, therefore, the major problem is to identify the genuine metabolites with fidelity.

We have now applied the FPT for the first time to MRS signals from malignant and benign ovarian lesions [14,15]. We chose this research area because of its critical clinical importance, since early ovarian cancer detection procures a major survival benefit, but the currently available methods have low diagnostic accuracy, due mainly to low specificity. Because of the small size and motion of this organ, in vivo MRS is severely hampered by problems of low resolution, while it is seen with in vitro MRS that a number of MR-observable compounds can help identify malignant adnexal lesions. We have shown that the Padé-optimization provides clearly superior resolution compared to the customary data analytical method, i.e., the FFT. We also have demonstrated how the FPT yields the unequivocal, exact parametric data needed to reconstruct the metabolite concentrations which characterize ovarian cancer and distinguish this from non-malignant samples. *These findings open an entirely new avenue for improving ovarian cancer diagnostics*. We have also begun investigations along these lines for breast and prostate cancer and melanoma using the FPT and certain preliminary results are described in [13]. Therein we also describe preliminary findings applying the FPT to magnetic resonance imaging (MRI), two-dimensional MRS and MRSI, with a particular focus on improved target definition for radiotherapy, dose planning and post-operative follow-up.

2 Theory

2.1 Benchmark reconstruction via Padé optimization of all parameters needed for reliable quantification of MRS signals

We have now performed studies showing that the FPT provides exact quantification of MRS signals and thereby metabolite concentrations are reliably and unequivocally obtained with an intrinsic and robust error analysis. In Refs. [5,9,12] validation is given for the powerful computational algorithms by which the FPT yields quantitative spectral parameters. This is done without fitting and the solution is *unique*. Further, the FPT outperforms other parametric estimators, e.g., the linear predictor (LP) [16], Hankel-Lanczos Singular Value Decomposition (HLSVD) [17], etc. Likewise, the FPT outperforms all fitting techniques used in MRS: Variable Projection Method (VARPRO) [18], Advanced Method for Accurate Robust and Efficient Spectral fitting (AMARES) [19], Linear Combination of Model in vitro Spectra (LCModel) [20], etc.

Confidence in the FPT is built systematically by considering theoretically generated as well as encoded free induction decays (FIDs).

2.2 Proof of the vital importance of quantum mechanics in signal processing

The textbook [12] provides advanced analysis of virtually all the significant signal processing methods. In particular, Ref. [12] establishes the theoretical criteria of what a reliable signal processor is (and especially also what it is not) supposed to be. Based upon such criteria, Ref. [12] has built the most practical algorithms for versatile applications, including those in MRS. These algorithms have now become widely used in such diverse disciplines as physics, chemistry, biology as well as medicine. This shows again and again that the correct theoretical basis is of primary importance to be established first, and with this accomplished, the ensuing implementations are bound to succeed. The main conclusion from Ref. [12] of paramount practical relevance is that for a successful application of *parametric* signal processing, the physics of the studied phenomenon must be accurately described by an appropriate mathematical model. This model can, in turn, be used to extract the parameters of the analyzed signal. Such reconstructed signal parameters are given by the unique set of nodal frequencies and amplitudes $\{\omega_k, d_k\}(k = 1, 2, 3, \ldots, K)$, as well as the order K of the underlying system (in MRS, K is the exact number of genuine resonances)[1]. This latter set of parameters holds the entire sought information, which then uncovers the *underlying dynamics and mechanisms that actually produced the encoded time signal*. What sets Ref. [12] apart from previous, related studies within MRS is a deep realization that signal processing, which has thus far been considered as a discipline on its own, is basically a part of a larger theoretical framework—the most successful physics theory: quantum mechanics. This sprang from the proof of the equivalence of the most generic time signals with the fundamental quantum-mechanical entities—the autocorrelation functions. Naturally, such a proof laid the basis for the most adequate physics (as per the above request)—quantum mechanics to spectrally analyze time signals. Equally naturally, this proper physics brought the correct mathematical model for signals: (i) autocorrelation functions and (ii) Green functions for the most adequate descriptions in the time and frequency domain, respectively.

Of critical importance is that such a dual mathematical modelling in the two complementary domains (time and frequency) is not imposed ad hoc or by some phenomenological set of procedures and recipes that are otherwise abundant in the MRS literature [18–20] and beyond. Rather, the mathematical model for any time signal and the corresponding spectrum emerges *uniquely* from the quantum dynamics of the investigated system.

This is the case because the dynamics, as the evolution in time, is rooted in the system's so-called dynamics operator, which is recognized in quantum mechanics as the time evolution operator, $U(t)$. For conservative systems, the Hamiltonians H, as the sum of kinetic and potential energy operators, are stationary. This means that the

[1] Each metabolite, being a molecule, can have more than one resonance.

time-dependent Schrödinger equations:

$$i\frac{\partial}{\partial t}\Phi(t) = H\Phi(t), \tag{1}$$

impose the unique form for $U(t)$ as the exponential operator:

$$U(t) = e^{-iHt}, \tag{2}$$

which governs the system's dynamics in the quantum-mechanical way. This enables us to find the non-stationary state $\Phi(t)$ of the examined system at any time t, if we know the system's initial state Φ_0 at $t = 0$ (determinism of quantum mechanics). The prescription for finding the state of the system is straight-forward and consists of applying the evolution operator $U(t)$ to Φ_0, to yield:

$$\Phi(t) = U(t)\Phi_0. \tag{3}$$

Of course, the Hamiltonian H, the initial state Φ_0 and, hence, the evolution operator $U(t)$ are all unknown prior to the analysis. However, these unknown quantum-mechanical entities are all ingrained in a single quantity called the auto-correlation function, $C(t)$. As its name indicates, $C(t)$ correlates the state of the system from one time instance to another, say from $t = 0$ [Φ_0] to $t \neq 0$ [$\Phi(t)$]. Intuitively and plausibly, the degree of correlation is the largest (smallest) for the maximum (minimum) overlap of $\Phi(t)$ and Φ_0. In quantum mechanics, such an overlap is determined by the scalar or inner product of $\Phi(t)$ with Φ_0, as symbolized via the projection of $|\Phi_0(t)\rangle$ onto $\langle\Phi_0|$, i.e., $\langle\Phi_0|\Phi(t)\rangle$. Thus, the auto-correlation function $C(t)$ is defined precisely by this latter overlap:

$$C(t) \equiv \langle \Phi_0 \,|\Phi(t)\,\rangle = \langle \Phi_0|\, U(t)\,|\Phi_0\rangle\,. \tag{4}$$

To obtain the explicit functional dependence of the auto-correlation function C upon t, one uses the *time-independent* Schrödinger equation as the *frequency* eigenvalue problem,

$$H\Psi_k = \omega_k\Psi_k \quad (k = 1, 2, \ldots, K). \tag{5}$$

Here, Ψ_k is the complete stationary state of the system and ω_k is the corresponding fundamental angular frequency ($\omega_k = 2\pi f_k$), where f_k is the associated linear frequency. One of the cornerstones of quantum mechanics is the statement of completeness, which asserts that everything which could possibly be learned about any system is contained in the set of the eigensolutions $\{\omega_k, \Psi_k\}$ of the above Schrödinger eigenvalue problem. In other words, once the set $\{\omega_k, \Psi_k\}$ becomes available, we have the entire information about the studied system. Conversely, if $\{\omega_k, \Psi_k\}$ are known, we can reconstruct the dynamics of the system via the so-called *spectral* representation/decomposition of

H or $U(t)$ as:

$$H = \sum_{k=1}^{K} \omega_k \pi_k, \tag{6}$$

and

$$U(t) = \sum_{k=1}^{K} \pi_k e^{-i\omega_k t}, \tag{7}$$

where π_k is the projection operator,

$$\pi_k = |\Psi_k\rangle \langle\Psi_k|, \quad \mathrm{Im}(\omega_k) < 0. \tag{8}$$

Hereafter, $\mathrm{Re}(u)$ and $\mathrm{Im}(u)$ denote the real and imaginary parts of a complex number u. Inserting this latter spectral representation for $U(t)$ into Eq. (4) yields, at once, the sought functional dependence of C upon t as:

$$C(t) = \sum_{k=1}^{K} d_k e^{-i\omega_k t}, \tag{9}$$

where

$$d_k = \langle\Phi_0|\Psi_k\rangle^2. \tag{10}$$

Hereafter, we use the symmetric version of the scalar product with no complex conjugation on either of the involved functions, i.e., $\langle f|g\rangle = \langle g|f\rangle$. Thus, the end result is the expression for the autocorrelation function $C(t)$ as a linear superposition of K damped complex exponentials. This coincides with the like and ubiquitous form of a generic time signal $c(t)$. *Hence, the equivalence of quantum-mechanical auto-correlation functions with time signals* $C(t) = c(t)$ [12,21,22]. Thus, we see that this latter mathematical model for a time signal, as a sum of damped complex exponentials, is imposed by quantum mechanics and, therefore, emboldens the entire information about the studied system (completeness statement of quantum mechanics, as stated above).

How does this quantum-mechanical signal processing compare with fitting e.g., an MRS signal to the same sum of damped complex exponentials as is customarily done in e.g., AMARES, LCModel and other least-square adjustable algorithms?

(i) The first, most dramatic and *clinically relevant difference* is the non-uniqueness of fitting, as opposed to the uniqueness of the quantum-mechanical prescription. Specifically, widely different combinations of the signal's parameters $\{\omega_k, d_k\}$ and their number K, can produce the same least-square type of fit to $c(t)$. Of course, such a situation is untenable in the clinical setting. By contrast, quantum

mechanics decomposes a given time signal $c(t)$ into a *unique* set of precisely K complex damped harmonics.

(ii) The second basic difference between fitting and quantum-mechanical signal processing is that the former has no natural relationships between ω_k and d_k, as opposed to the latter where d_k is given by Eq. (10), with ω_k being implicitly present via Ψ_k. The implication of this difference is that fitting tries to adjust d_k and ω_k independently of each other, while minimizing the error, such that wide variations in e.g., ω_k can be largely compensated by equally wide variations in d_k thus inevitably leading to non-unique estimates. By contrast, d_k from quantum mechanics is constrained to obey a particular relationship (10) which, as we saw, emerges from the first principles of physics. We have shown in Ref. [12] that it is this latter constraint on d_k which guarantees the uniqueness of the quantum-mechanically reconstructed spectral amplitudes $\{d_k\}$ for the corresponding set $\{\omega_k\}$ of the fundamental frequencies that are also retrieved uniquely. Moreover, the model order K, or equivalently, the number of resonances, is also reconstructed exactly in quantum mechanics, in contradistinction to guessing, as germane to all the fitting routines used in MRS (LCModel, AMARES, VARPRO, etc). In this way, quantum mechanics provides us with the possibility of the exact extraction of all the spectral frequencies and amplitudes of all the genuine metabolites, as well as their true number. The key clinical ramification of this latter feature is the unique, and, hence, the most reliable quantification of all the physical metabolite concentrations.

Once the time signal's parameters $\{\omega_k, d_k\}(1 \leq k \leq K)$ have become available, the corresponding spectrum is automatically given by the Green function in the Heaviside partial fraction decomposition:

$$G(\omega) = \sum_{k=1}^{K} \frac{d_k}{\omega - \omega_k}. \tag{11}$$

The r.h.s. of this equation can explicitly be summed up to give the unique polynomial quotient $P_{K-1}(\omega)/Q_K(\omega)$, which is recognized as the so-called para-diagonal FPT. This shows that the FPT *is* the algorithm of quantum mechanics and, as such, is the method of choice for spectral analysis of generic time signals, including those from MRS. Time-frequency duality implies that the inverse FPT computed from the Padé spectrum P_{K-1}/Q_K will yield the time signal $c(t)$ as a sum of K damped complex exponentials. This determines that the optimal mathematical model for the frequency spectrum of these time signals is prescribed quantum-mechanically, to be the ratio of two polynomials, i.e., the FPT. In other words, just as in the time domain where quantum mechanics predicts the form of the time signal as the sum of damped exponentials, by virtue of the time-frequency dual representation, the same physics automatically prescribes that the frequency spectrum is given by the Padé quotient of two polynomials. *This is the origin of the subsequently revealed unprecedented algorithmic success of the FPT, via its demonstrable, exact reconstructions*, as shown in Refs. [6,7].

3 Results

3.1 The fast Padé transform: specific achievements in quantification of MRS signals

We have noted that there is an urgent need for accurate quantification to determine metabolite concentrations, so that MRS can be better used to detect and characterize cancers, with clear distinction from non-malignant processes. Metabolite concentrations can only be accurately computed if the spectral parameters are obtained in a reliable way with an adequate error analysis, accompanied by the ability to clearly identify and thereby separate noise from the physical signal. This is uniquely provided by the FPT.

The recent study [5] represents a critical step forward for signal processing in MRS, with particular relevance to clinical oncology, due to the unprecedented capability of the FPT to unambiguously resolve and quantify all the physical resonances.

We have performed computations [5,6] using the FPT to reconstruct spectral parameters for time signals that closely match FIDs encoded on clinical scanners via proton MRS from the brain of a healthy volunteer [23,24]. Included in this successful reconstruction are not only isolated and closely overlapping resonances, but also those which are nearly degenerate. These latter resonances cannot be possibly even detected via the total shape spectrum or error analysis. Only the powerful and accurate parametric analysis provided e.g., by FPT can detect and also exactly quantify such resonances, which, as discussed, are often of major clinical importance.

In Table 1 adapted from Ref. [5] we present the reconstructed spectral parameters from the FPT at five partial signal lengths ($N/32 = 32$, $N/16 = 64$, $N/8 = 128$, $N/4 = 256$ and $N/2 = 512$) and at the full signal length ($N = 1024$). The left column of Table 1 through panels (i), (ii) and (iii) shows the parameters of the found 10, 14 and 20 resonances at $N/32 = 32$, $N/16 = 64$, $N/8 = 128$, respectively. The results for these detected 10, 14 and 20 resonances from panels (i), (ii) and (iii) are only approximations to the corresponding exact input values of the spectral parameters [that coincide with the right column of Table 1, panels (iv), (v) and (vi)]. This is due to relatively small numbers of signal points employed ($N/M \leq 128$). The right column of Table 1 via panels (iv), (v) and (vi) shows the spectral parameters retrieved at $N/4 = 256$, $N/2 = 512$ and $N = 1{,}024$, respectively.

It has been demonstrated in Refs. [5,8] that for a quarter ($N/4 = 256$) of the full signal length N, the FPT was able to reconstruct all 25 resonances with the exact values for each of their spectral parameters. Stunningly, these values remain completely stable when convergence is passed with further signal points included, as shown in panels (v) and (vi) of Table 1. This is due to the pole-zero cancellation, or equivalently, Froissart doublets, presented in the next section. Achieving convergence represents the "signature of reconstruction" of the true number K of resonances. Further increase of K does not change the converged result for the Padé spectrum in the FPT.

These points are also graphically illustrated in Fig. 1, in which it is seen that the estimated parameters via the FPT are employed to construct the absorption component spectrum (left panels) and this is compared to the total shape spectrum (right panels). While the shape (or envelope) spectrum has converged at the partial signal

Table 1 Numerical values of the spectral parameters (position $\mathrm{Re}(f_k^-)$, width $\mathrm{Im}(f_k^-)$ and height $d_k^- = |d_k^-|$, all phases of d_k^-'s set to zero) from a time signal reminiscent of an encoded FID via MRS from human brain at the magnetic field strength $B_0 = 1.5\,\mathrm{T}$ [23]. These parameters are reconstructed by solving the quantification problem at different signal lengths [$N/32 = 32$ (i), $N/16 = 64$ (ii), $N/8 = 128$ (iii), $N/4 = 256$ (iv), $N/2 = 512$ (v), and $N = 1024$ (vi)], using the variant FPT $^{(-)}$of the fast Padé transform with the initial convergence region outside the unit circle. Convergence is achieved at $N/4 = 256$, and remains stable at longer signal lengths. Adapted from Ref. [5]. Hereafter, arbitrary units are abbreviated as au and parts per million as ppm

CONVERGENCE OF SPECTRAL PARAMETERS in the FAST PADE TRANSFORM, FPT$^{(-)}$: SIGNAL LENGTH N/M, N=1024, M=1–32

Peak #	Position (ppm)	Width (ppm)	Height (au)
1	1.010	0.206	0.223
3	1.514	0.421	0.251
4	1.642	0.097	0.039
6	2.065	0.069	0.340
12	2.638	0.276	0.423
15	3.054	0.138	0.414
17	3.377	0.037	0.017
23	3.972	0.113	0.230
24	4.092	0.086	0.089
25	4.681	0.135	0.111

(i) N/32 = 32: Position $\mathrm{Re}(f_k^-)$, Width $\mathrm{Im}(f_k^-)$, Height d_k^-

Peak #	Position (ppm)	Width (ppm)	Height (au)
1	0.989	0.180	0.130
2	1.121	0.241	0.148
3	1.562	0.207	0.195
5	2.029	0.012	0.026
6	2.055	0.071	0.376
9	2.475	0.194	0.315
10	2.589	0.054	0.060
15	3.058	0.051	0.161
16	3.237	0.071	0.178
19	3.564	0.045	0.035
21	3.778	0.068	0.075
22	3.941	0.048	0.087
24	4.269	0.055	0.016
25	4.680	0.136	0.113

(ii) N/16 = 64: Position $\mathrm{Re}(f_k^-)$, Width $\mathrm{Im}(f_k^-)$, Height d_k^-

Peak #	Position (ppm)	Width (ppm)	Height (au)
1	0.985	0.180	0.122
2	1.112	0.256	0.160
3	1.546	0.169	0.123
4	1.704	0.133	0.051
5	2.013	0.073	0.347
6	2.044	0.043	0.330
7	2.156	0.036	0.039
9	2.351	0.015	0.007
10	2.510	0.130	0.200
12	2.654	0.049	0.061
13	2.808	0.018	0.001
15	3.072	0.053	0.184
16	3.231	0.078	0.207
17	3.366	0.036	0.011
19	3.588	0.021	0.024
20	3.700	0.042	0.047
21	3.803	0.027	0.037
22	3.944	0.045	0.084
24	4.271	0.055	0.016
25	4.680	0.136	0.113

(iii) N/8 = 128: Position $\mathrm{Re}(f_k^-)$, Width $\mathrm{Im}(f_k^-)$, Height d_k^-

Peak #	Position (ppm)	Width (ppm)	Height (au)
1	0.985	0.180	0.122
2	1.112	0.257	0.161
3	1.548	0.172	0.135
4	1.689	0.118	0.034
5	1.959	0.062	0.056
6	2.065	0.031	0.171
7	2.145	0.050	0.116
8	2.261	0.062	0.092
9	2.411	0.062	0.085
10	2.519	0.036	0.037
11	2.676	0.033	0.008
12	2.676	0.062	0.063
13	2.855	0.016	0.005
14	3.009	0.064	0.065
15	3.067	0.036	0.101
16	3.239	0.050	0.096
17	3.301	0.064	0.065
18	3.481	0.031	0.011
19	3.584	0.028	0.036
20	3.694	0.036	0.041
21	3.803	0.024	0.031
22	3.944	0.042	0.068
23	3.965	0.062	0.013
24	4.271	0.055	0.016
25	4.680	0.136	0.113

(iv) N/4 = 256: Position $\mathrm{Re}(f_k^-)$, Width $\mathrm{Im}(f_k^-)$, Height d_k^-

Peak #	Position (ppm)	Width (ppm)	Height (au)
1	0.985	0.180	0.122
2	1.112	0.257	0.161
3	1.548	0.172	0.135
4	1.689	0.118	0.034
5	1.959	0.062	0.056
6	2.065	0.031	0.171
7	2.145	0.050	0.116
8	2.261	0.062	0.092
9	2.411	0.062	0.085
10	2.519	0.036	0.037
11	2.676	0.033	0.008
12	2.676	0.062	0.063
13	2.855	0.016	0.005
14	3.009	0.064	0.065
15	3.067	0.036	0.101
16	3.239	0.050	0.096
17	3.301	0.064	0.065
18	3.481	0.031	0.011
19	3.584	0.028	0.036
20	3.694	0.036	0.041
21	3.803	0.024	0.031
22	3.944	0.042	0.068
23	3.965	0.062	0.013
24	4.271	0.055	0.016
25	4.680	0.136	0.113

(v) N/2 = 512: Position $\mathrm{Re}(f_k^-)$, Width $\mathrm{Im}(f_k^-)$, Height d_k^-

Peak #	Position (ppm)	Width (ppm)	Height (au)
1	0.985	0.180	0.122
2	1.112	0.257	0.161
3	1.548	0.172	0.135
4	1.689	0.118	0.034
5	1.959	0.062	0.056
6	2.065	0.031	0.171
7	2.145	0.050	0.116
8	2.261	0.062	0.092
9	2.411	0.062	0.085
10	2.519	0.036	0.037
11	2.676	0.033	0.008
12	2.676	0.062	0.063
13	2.855	0.016	0.005
14	3.009	0.064	0.065
15	3.067	0.036	0.101
16	3.239	0.050	0.096
17	3.301	0.064	0.065
18	3.481	0.031	0.011
19	3.584	0.028	0.036
20	3.694	0.036	0.041
21	3.803	0.024	0.031
22	3.944	0.042	0.068
23	3.965	0.062	0.013
24	4.271	0.055	0.016
25	4.680	0.136	0.113

(vi) N = 1024: Position $\mathrm{Re}(f_k^-)$, Width $\mathrm{Im}(f_k^-)$, Height d_k^-

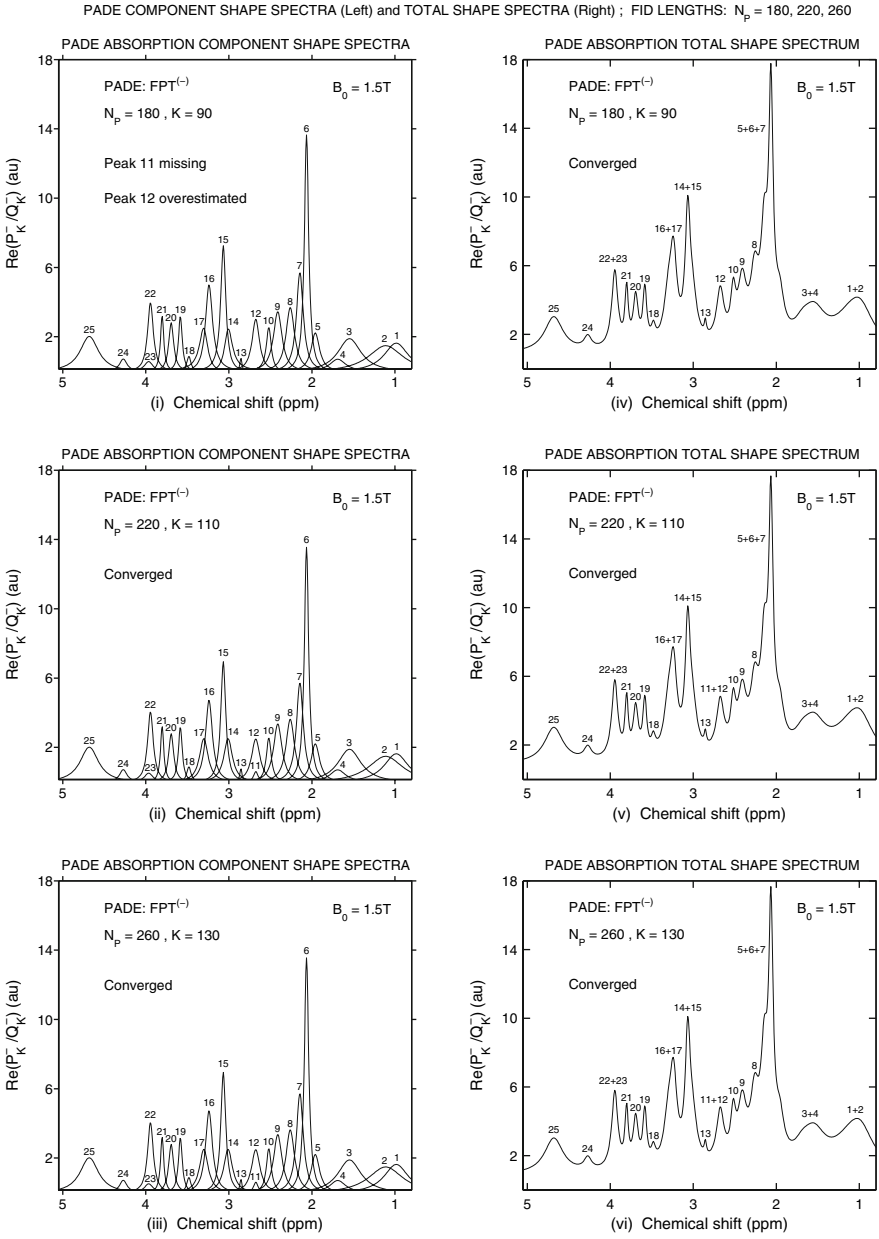

Fig. 1 Absorption component shape spectra reconstructed by the FPT$^{(-)}$ from a time signal reminiscent of an encoded FID via MRS from human brain at the magnetic field strength $B_0 = 1.5\,T$ [23] for each resonance (left) and their sums as total shape spectra (right). The displayed results correspond to three different partial signal lengths $N_P = 180$, 220 and 260. Total shape spectra at $N_P = 180$ on panel (iv) converge despite the missing peak #11 and the related overestimate of peak #12. Adapted from Ref. [5]

length, $N_P = 180$ (top right panel), this is not the case for the component spectrum.[2] As seen on the top left panel of Fig. 1 at the partial signal length $N_P = 180$, peak # 12 is overestimated whereas peak # 11 is missing. It is at the partial signal length $N_P = 220$ [middle left panel (ii)] that the very small peak #11 is first detected and the component shape spectrum has converged. This is also shown in [13] which provides a generic illustration of the importance of obtaining a component shape spectrum *prior* to the total shape spectrum, as opposed to fitting which tries to uncover the component spectra underneath a given total shape spectrum.

3.1.1 Machine accurate quantification of magnetic resonance spectroscopic signals with Padé optimization

In Ref. [25], we performed further computations using the FPT to reconstruct spectral parameters for an MRS time signal that closely matches FIDs encoded via proton MRS from the brain of a healthy volunteer [23,24]. Therein it is demonstrated that at full convergence ($N_P = 220$), the exact numerical values of all the fundamental frequencies and amplitudes $\{f_k, d_k\}$ are reconstructed to 12 given decimal places. This confirms the achievement of machine accuracy (i.e., exact computer-wise) in the reconstruction of the spectral parameters, from which metabolite concentrations are then obtained.

In Table 2, we present the reconstructed spectral parameters at the two partial signal lengths, $N_P = 180$ and $N_P = 220$, by reference to [25]. Therein, it is seen that at the signal length $N_P = 220$, full numerical convergence is attained to 12 digits of accuracy.

Detailed numerical analyses from Refs. [5,8] reveal that these 12 digits of accuracy are stable (by virtue of Froissart doublets; see later on) at longer signal lengths: $N/4 = 256$, $N/2 = 512$ and $N = 1024$. This further confirms the reliability of the FPT for analysis of MR time signals, in contrast to other parametric estimators, which are typically unstable as a function of signal length for a given bandwidth. In Ref. [7], we demonstrate and explain in detail, why mathematical methods through Padé-optimization of MRS can indeed play a decisive role in early cancer diagnostics, in particular by detecting and quantifying overlapping resonances that often are the most critical for identifying malignancy [26,27].

Thus, these benchmark studies have now been performed in which the FPT was shown to provide exact quantification of MRS signals and thereby metabolite concentrations are reliably and unequivocally obtained with the accompanying error analysis of proven validity. Together with the practical implementation described in [13], a valid and exact approach to quantification of MRS signals has now been achieved. Via this type of implementation, Padé-optimization MRS is expected soon to become a standard diagnostic tool for clinical oncology.

[2] The displayed numbers of the component peaks on the converged component shape spectra (panels 2 & 3) correspond to the following metabolites: 1–4 (mobile lipids), 5 (Gaba), 6 (NAA), 7 (NAAG), 8 (Gaba), 9 (Glutamate), 10 (Glutamine), 11 (Aspartate), 12 (NAA), 13 (Aspartate), 14 (Creatine), 15 (Phosphocreatine), 16 (Choline), 17 (Phosphocholine), 18 (Taurine), 19 (Myoinositol), 20 (Glutamate), 21 (Glutamine), 22 (Creatine), 23 (Phosphocreatine), 24 (Phosphocholine), 25 (Water). For a graphic map of metabolite assignments corresponding to MRS from normal human brain, see [13].

Table 2 Reconstruction of numerical values of the input complex frequencies and amplitudes $\{f_k^-, d_k^-\}$ using the FPT$^{(-)}$ at two partial FID lengths, $N_P = 180$ and 220. All the phases in the input parameters d_k are set to zero so that $d_k = |d_k|$. The input FID is defined by $c_n = \sum_{k=1}^{K} d_k \exp(2in\pi\tau f_k)(\mathrm{Im} f_k > 0)$ where $K = 25$ and τ is the sampling time. Headings $X_{N_P}(X = A, B, C; N_P = 180, 220)$ denote the number of exact digits in the Padé-reconstructed spectral parameters. The minus signs in the 11th row of columns $X_{180}(X = A, B, C)$ indicate that the 11th peak is missing in the reconstruction at $N_P = 180$. Columns $X_{220}(X = A, B, C)$ show that using only 220 FID points out of 1024 sampled input data, the FPT$^{(-)}$ retrieves exactly all the spectral parameters with their original 12 digit accuracy for the 25 peaks, including the two near degenerate real frequencies (peaks 11 and 12) that are separated by an infinitesimally small splitting (10^{-11} ppm). Here, A, B, C relate to Re(f_k), Im(f_k) and $|d_k|$, respectively. Adapted from Ref. [25].

Proof-of-principle accuracy of FPT$^{(-)}$ for quantification in MRS; partial FID lengths: $N_P = 180, 220$

n_k^o	Re(f_k) (ppm)	A_{180}	A_{220}	Im(f_k) (ppm)	B_{180}	B_{220}	$\|d_k\|$ (au)	C_{180}	C_{220}
1	0.98502379048	5	12	0.17990702201	6	12	0.12201338573	5	12
2	1.11200690857	5	12	0.25659054387	5	12	0.16102301354	4	12
3	1.54801482971	5	12	0.17204537140	5	12	0.13503330578	4	12
4	1.68903176043	4	12	0.11770166604	6	12	0.03401254085	6	12
5	1.95901160274	4	12	0.06238018044	5	12	0.05600424857	4	12
6	2.06502407981	4	12	0.03125260267	5	12	0.17102358306	4	12
7	2.14500270476	4	12	0.05002544195	3	12	0.11603368953	3	12
8	2.26101532905	4	12	0.06237934902	3	12	0.09202335049	3	12
9	2.41102150732	4	12	0.06237422557	3	12	0.08501750894	3	12
10	2.51903027327	3	12	0.03599412378	4	12	0.03700259438	4	12
11	2.67601690282	-	12	0.03282539014	-	12	0.00803536496	-	12
12	2.67601690283	4	12	0.06237759999	2	12	0.06301390467	2	12
13	2.85502705876	3	12	0.01612538422	3	12	0.00502635089	4	12
14	3.00901406482	3	12	0.06391077363	3	12	0.06503575473	2	12
15	3.06703685438	3	12	0.03599492238	3	12	0.10101269056	2	12
16	3.23902878775	3	12	0.05002202198	3	12	0.09600757431	2	12
17	3.30101387656	2	12	0.06390293515	3	12	0.06502706396	2	12
18	3.48103205784	3	12	0.03106596433	3	12	0.01101319057	3	12
19	3.58401389769	4	12	0.02821228070	4	12	0.03603204548	3	12
20	3.69403557653	4	12	0.03632802757	5	12	0.04101607586	4	12
21	3.80302402567	4	12	0.02390558758	4	12	0.03102656032	4	12
22	3.94401303293	4	12	0.04153226854	3	12	0.06800389846	3	12
23	3.96503686091	3	12	0.06237504151	3	12	0.01303609434	3	12
24	4.27101589852	6	12	0.05493585133	6	12	0.01601376287	7	12
25	4.68000000000	7	12	0.13614250986	7	12	0.11302657043	6	12

3.2 Signal–Noise Separation (SNS): reliable procedure for separating physical from non-physical (noise) information in MRS

In Ref. [6], we have validated a powerful means of determining whether a given reconstructed resonance is true or spurious. This is done by computing a sequence of the Padé shape spectra $\{P_m/Q_m\}(m = 1, 2, 3, \ldots)$ in the frequency range of interest, say 0.5–5 ppm. Here, the fingerprint of detection of the exact number K of resonances is the attainment of the stabilization value $m = m'$ after which a saturation is systematically maintained by observing that $P_{m'+q}/Q_{m'+q} = P_{m'}/Q_{m'}$ $(q = 1, 2, 3, \ldots)$. This critical transition $(m = m')$ yields the sought K as $K = m'$, which has been verified

to work in practice with MRS signals [6]. This is the concept of Froissart doublets, or equivalently, pole-zero cancellations [5,6,28].

Specifically, the computation is carried out by gradually and systematically increasing the degree of the Padé polynomials. As these degrees change, the reconstructed spectra fluctuate until stabilization occurs. The value of the polynomial degree at which the predetermined level of accuracy is achieved represents the sought exact number of resonances K. This constancy of the reconstructed values can be obtained, e.g., via the cannonical representation of the Padé polynomial quotients:

$$\frac{P^{\pm}_{K-1}(z^{\pm 1})}{Q^{\pm}_{K}(z^{\pm 1})} = \frac{p^{\pm}_{K-1}}{q^{\pm}_{K}} \frac{\prod_{k=1}^{K-1}(z^{\pm 1} - \tilde{z}^{\pm}_{k})}{\prod_{k'=1}^{K}(z^{\pm 1} - z^{\pm}_{k'})}, \tag{12}$$

where $\tilde{z}^{\pm}_{k}$ and $z^{\pm}_{k}$ are the zeros of $P^{\pm}_{K-1}$ and $Q^{\pm}_{K}$, respectively. The quotient form from (12) leads to cancellation of all the terms in the Padé numerator and denominator polynomials, when the computation is continued after the stabilized value of the order in the FPT has been attained, so that:

$$\frac{P^{\pm}_{K-1+m}(z^{\pm 1})}{Q^{\pm}_{K+m}(z^{\pm 1})} = \frac{P^{\pm}_{K-1}(z^{\pm 1})}{Q^{\pm}_{K}(z^{\pm 1})}, \quad (m = 1, 2, 3, \ldots). \tag{13}$$

The Cauchy residue of $P^{\pm}_{K-1}/Q^{\pm}_{K}$ from (12) represents the amplitudes $d^{\pm}_{k}$ whose analytical expressions are:

$$d^{\pm}_{k} = \frac{p^{\pm}_{K-1}}{q^{\pm}_{K}} \frac{\prod_{k'=1}^{K-1}(z^{\pm 1}_{k} - \tilde{z}^{\pm}_{k'})}{\prod_{k'=1,k'\neq k}^{K}(z^{\pm 1}_{k} - z^{\pm}_{k'})}. \tag{14}$$

Therefore, it is obvious from (14) that whenever $z^{\pm}_{k} = \tilde{z}^{\pm}_{k}$, the amplitudes $d^{\pm}_{k}$ of the poles from the Froissart doublets are exactly zero:

$$d^{\pm}_{k} = 0 \quad \text{for} \quad z^{\pm}_{k} = \tilde{z}^{\pm}_{k}. \tag{15}$$

Figure 2 shows the result for a noise-corrupted MR time signal. Therein, Gauss-distributed zero mean noise was added with a standard deviation $\sigma = 0.00289$ root-mean-square of the noiseless FID. The number 0.00289 is approximately 1.5% of the height of the weakest resonance in the spectrum (#13 aspartate at 2.855 ppm), and this is considered quite realistic for encoded data with good signal-to-noise ratio (SNR), as well as being sufficient to illustrate the principles of Froissart doublets. Higher noise levels, up to 100% of the height of the weakest resonance have also been examined and the Froissart concept is found to hold in those cases, as well. In the "noisy" case from Fig. 2, there was a total of 128 resonances, 103 of which were spurious. Using the FPT$^{(+)}$, all the Froissart doublets were clearly identified by pole-zero cancellation and with their imaginary components of the frequencies being negative and the corresponding zero-valued amplitudes. The 25 genuine resonances were all exactly reconstructed at one-quarter of the total signal length ($N/4 = 256$) with the imaginary

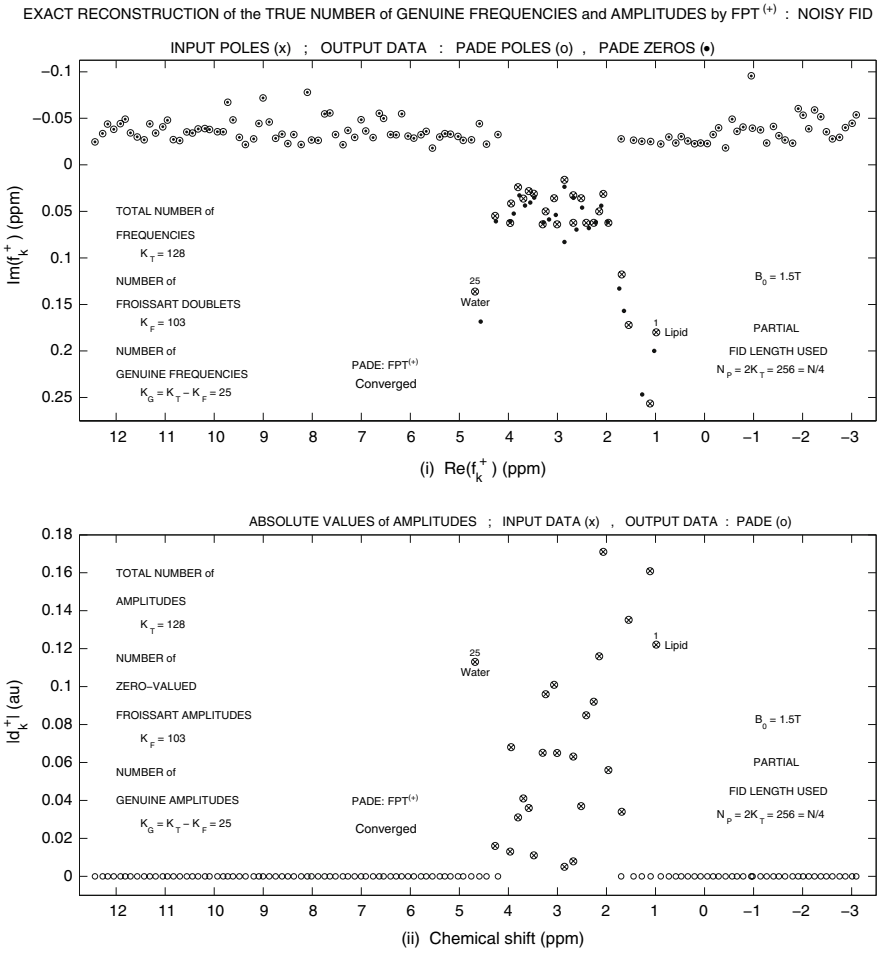

Fig. 2 Use of Froissart doublets to unequivocally extract the exact number K_G of genuine frequencies and amplitudes from the total number $K_T \equiv K$ of the spectral parameters reconstructed by the FPT$^{(+)}$ for the *noise-corrupted* time signal. The FPT$^{(+)}$ separates the genuine from the spurious frequencies in the two non-overlapping regions, $\mathrm{Im}(f_k^+) > 0$ and $\mathrm{Im}(f_k^+) < 0$, respectively. All the spurious (Froissart) amplitudes are also identified by their zero values. Adapted from Ref. [6]

component of the frequencies being positive [top panel (i) of Fig. 2]. In the bottom panel (ii) of Fig. 2, it is seen that all the spurious (Froissart) amplitudes are equal to zero, while the absolute values of the amplitudes are non-zero for the true resonances.

More specifically, in Fig. 2, we give the Argand diagram for complex frequencies.[3] In this figure, we illustrate the concept of Froissart doublets for a synthesized FID derived from realistic MRS data encoded at 1.5 T (the same as was used in Table 1 and Fig. 1). We use the form of the FPT with its convergence region inside the unit

[3] In general, an Argand plot for a given complex quantity shows the variation of the imaginary versus real part of that quantity. It is a very useful concept which is extensively used in physics and chemistry.

circle, namely FPT$^{(+)}$ [3,12]. After convergence has been reached, there is a total of 128 resonances, but only 25 of these are genuine. The remaining 103 are spurious resonances. The top panel (i) in Fig. 2 shows that all these spurious resonances are Froissart doublets, namely that the poles stemming from the denominator polynomial, marked as open circles automatically coincide with the corresponding zeros of the numerator polynomial denoted by small filled circles (dots). This is a graphic representation of pole-zero cancellation. In contrast, there are 25 tightly-packed genuine resonances. In the case of the FPT$^{(+)}$, all the imaginary parts of the genuine and spurious frequencies are positive and negative, respectively. Thereby, the genuine chemical shifts between 0.985 and 4.68 ppm are clearly separated from the spurious resonances.

In the bottom panel (ii) of Fig. 2, it can be seen that all the spurious resonances have amplitudes equal to zero, as per (15). At one-quarter of the total signal length ($N/4 = 256$) for the 25 true reconstructed resonances the absolute values of the amplitudes are all seen to have non-zero values. Moreover, these exactly coincide with the input data, since full convergence has been achieved at this signal length. The spurious resonances appear in all the parametric estimators that must use more than twice the number of unknown frequencies and amplitudes. This leads to an over-determined system which yields more resonances than the actual number present in the analyzed signal. The extra resonances are spurious and act as "noise" or are "noise-like. The problem is to identify these and then discard them. Among all the estimators, only the FPT can achieve this task with certainty, and this is done through the concept of the Froissart doublets, which acts as a powerful filter of spurious "noisy" or "noise-like" resonances, as illustrated in Fig. 2. Therefore, such an application of the Froissart doublets can be viewed as the introduction of a special filter, thereafter termed the Froissart filter.

Overall, the fast Padé transform is shown to resolve and quantify tightly overlapped and even nearly degenerate resonances that are abundantly seen in MR spectra generated using encoded in vivo time signals. Crucially, in the FPT, pole-zero cancellation (Froissart doublets) can be used to unequivocally distinguish true and spurious resonances. This is demonstrated not only in the noise-free case [13], but also for synthesized MR time signals corrupted by noise [6] at a level similar to realistic encoding conditions (Fig. 2).

Distinction of genuine from spurious peaks has been one of the thorniest challenges to MRS. The number of spurious resonances is always several times greater than the true metabolites. To reemphasize, in the present study there were 128 resonances, but only 25 were genuine. Thus, 103 or over 80% were spurious. It is obviously an essential precondition for trustworthy clinical applications of MRS that the genuine information be clearly and unambiguously identified. In recent studies [6,25] via the powerful concept of Froissart doublets (pole-zero cancellations) [28], the FPT has been shown to achieve this task. Here we have demonstrated that all the spurious resonances are clearly and unequivocally separated from the true metabolites, in the presence of noise as typically encountered in clinically encoded time signals with good SNR. These findings offer the solution to one of the most difficult problems hampering wider implementation of MRS in clinical oncology. The same problem of separation of genuine from spurious information in experimental data is present everywhere else,

whenever dealing with time signals encoded by all the other measuring methods, e.g., ion-cyclotron resonance mass spectroscopy (ICR-MS) [29], etc.

We now turn our attention to how these advantages of the FPT through clear identification of genuine spectroscopic information are of direct clinical relevance for cancer diagnostics.

3.3 Application of the FPT to MRS data derived from cancerous & benign ovarian fluid

We have performed initial studies [14,15] applying the FPT using data derived from benign and malignant ovarian cyst fluid encoded at high magnetic fields in vitro [30]. In these papers, we first presented a comprehensive, systematic review of the literature and concluded that this avenue is of clinical urgency for early ovarian cancer detection, a goal which is still elusive and achievement of which would confer a major survival benefit.

For the benign case, we derived the input data for the spectral parameters from those reported for median concentrations C_{met} (expressed in μmol/L) of twelve metabolites that were characteristic of benign ovarian cyst fluid [30]. These median values were obtained from 23 patients with benign ovarian cysts collected by Boss et al. [30]. Likewise, malignant concentrations correspond to the median values for malignant ovarian cysts from 12 patients [30], and these are used as the input data for the malignant case.

Via the FPT, fully converged shape spectra were obtained using only $N/16 = 64$ signal points. This is shown in Fig. 3, for the benign case [top right panel (iii)] and malignant case [bottom right panel (iv)]. In sharp contradistinction, the spectra generated using the FFT at the latter signal length are completely uninterpretable [top left panel (i), benign case; bottom left panel (ii), malignant case].

Figure 4 provides an in-depth comparison of the FPT and the FFT with respect to convergence of the absorption spectra at varying signal lengths with a fixed bandwidth for the FID which was derived from the malignant ovarian cyst data. The top two panels present the absorption spectra of the FPT at $N/32 = 32$ [left, (i)] and $N/16 = 64$ [right, (ii)]. At $N/32 = 32$ on panel (i), nine of the twelve metabolites are detected and identified. The remaining three resonances require 64 signal points to be quantitatively identified on panel (ii). At this latter signal length, all the peak heights are correct, and, in agreement with Table 3, at $N/16 = 64$, the absorption spectrum is fully converged in the FPT. The middle two panels show the performance for shape estimation by the FFT at the same two short signal lengths as in the FPT. In sharp contrast to the FPT, these FFT-generated spectra at $N/32 = 32$ [left, (iii)] and $N/16 = 64$ [right, (iv)] where $N = 1024$, are rough and uninterpretable. Full convergence of the absorption spectrum from the FFT requires sampling the FIDs with $N = 32\,\text{K} = 32768$ signal points and zero-filling to 64 K [bottom right panel, (vi)]. Here, K denotes kilobytes, $\text{K} = 1024$. The bottom left panel (v) of Fig. 4 shows the performance of the FFT at $N = 8\,\text{K} = 8192$, where the 12 resonances are resolved, but their peak heights are not all correct. This means that some of the metabolite concentrations from the FFT are still insufficiently accurate even at $N = 8\,\text{K}$. Moreover, it is seen in the Fourier panel (v) from Fig. 4 that the threonine, lactate and alanine resonances in the range 1.30–1.55 ppm have their baseline distorted relative to the converged spectra from panels

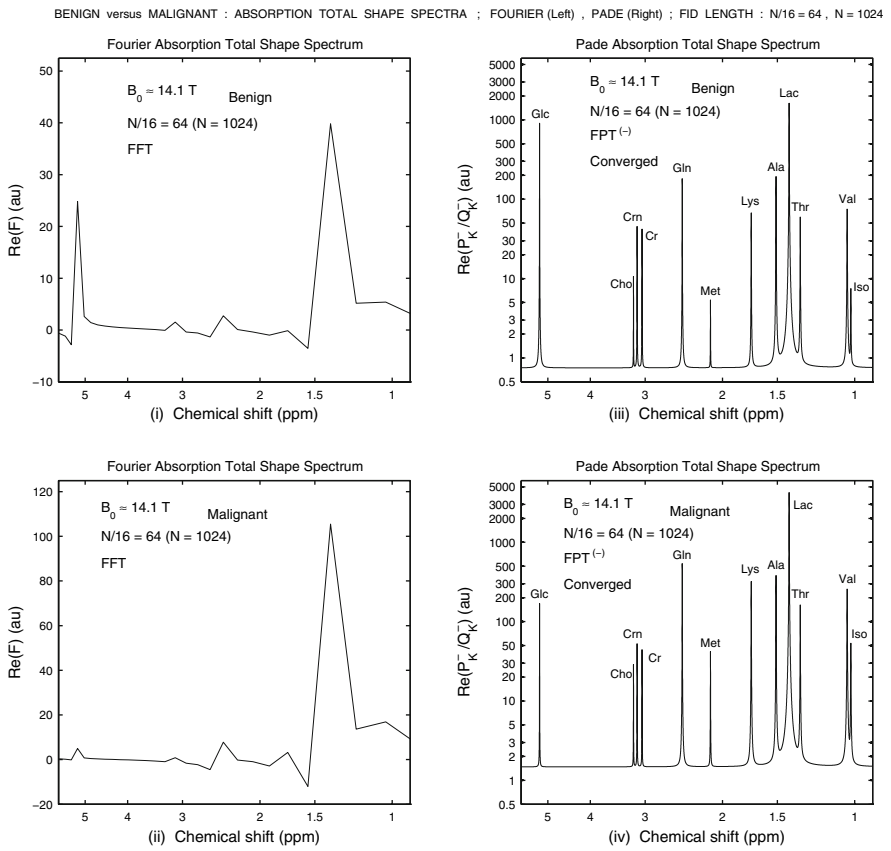

Fig. 3 Absorption spectra for cases derived from benign and malignant ovarian cyst MRS in vitro encoded data from Ref. [30]. Top panels compare the performance of the FFT [left (i)], FPT [right (iii)] at $N/16 = 64$ where $N = 1024$ for the benign case. The FPT is fully converged, but the corresponding FFT-generated spectra are uninterpretable. A similar pattern is seen in the malignant case [bottom panels, FFT [left (ii), FPT (right (iv)]. Adapted from Refs. [14,15]

(ii) (FPT) and (vi) (FFT). Note that the FPT does not use zero filling at all, whereas the FFT does [each of the Fourier panels (iii)–(vi) was obtained by one zero filling], i.e., doubling the nominal signal length $N/M (M > 1)$ by padding N/M zeros.

The numerical results are shown in Table 3. We found that the FPT reconstructed exactly all the input spectral parameters using very small fractions of the time signals. It is particularly striking to note in this clinically-relevant context that for the peak amplitudes (d_k) and line-width ($\mathrm{Im}\, f_k$) from which the metabolite concentrations are calculated, six digits of accuracy were required and achieved in this illustration to benchmark the FPT.

A substantial number of MR-observable compounds were found to distinguish between benign and cancerous ovarian lesions in Ref. [30]. Notably, concentrations of adjacent resonances such as threonine (1.33 ppm), lactate (1.41 ppm) and alanine (1.51 ppm) and the nearly overlapping resonances isoleucine and valine in the region

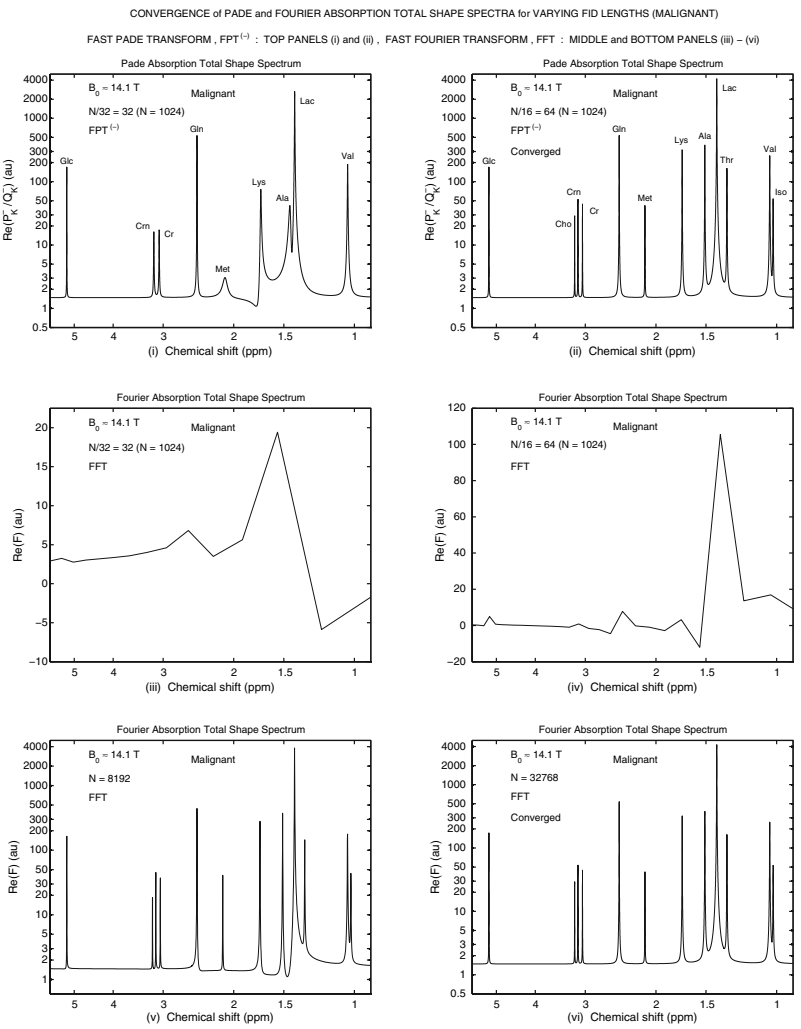

Fig. 4 Comparison of the FPT and the FFT with respect to convergence of the absorption spectra at varying fractions of the full signal length for the cases derived from malignant ovarian cyst MRS in vitro data encoded by Boss et al. [30] with a high resolution NMR 600 MHz spectrometer. ($B_0 = 14.1$ T). The top two panels present the absorption spectra of the FPT at $N/32 = 32$ [left, (i)] and $N/16 = 64$ [right, (ii)], where $N = 1024$. At $N/32 = 32$, nine of the 12 resonances are identified; the remaining three resonances require 64 signal points to be identified. At $N/16 = 64$, the peak heights are all correct and the total absorption shape spectrum is fully converged using the FPT. The middle two panels, (iii) and (iv), show the performance of the FFT at these same two partial signals lengths ($N/32$, $N/16$; $N = 1024$). In sharp contrast to the FPT, these FFT-generated spectra at $N/32 = 32$ and $N/16 = 64$ are rough, and uninterpretable. Full convergence of the absorption spectrum is achieved with the FFT at $N = 32\,\mathrm{K} = 32768$ signal points [bottom right panel, (vi)], where K denotes kilobyte, K = 1024. The bottom left panel (v) shows the performance of the FFT at $N = 8\,\mathrm{K} = 8192$, where the twelve resonances are resolved, but not with all the correct peak heights. Moreover, the baseline in the range 1.30–1.55 ppm is distorted relative to the converged spectra on panels (ii) (FPT) and (vi) (FFT). The FPT uses the original signal points with no zero filling. By contrast, all the displayed results from the FFT are obtained by doubling the quoted FID length with zero filling, as usual. Adapted from Ref. [14]

Table 3 Input and Padé-reconstructed data from FIDs derived from in vitro MRS time signals as encoded from benign and malignant ovarian cyst fluid [30]. Here, $\mathrm{Im}(f_k)$ (as the imaginary part of f_k) is proportional to the full width at half maximum (FWHM). The inverse $1/\mathrm{Im}(f_k)$ is proportional to the relaxation time T_{2k} of the kth resonance. Panel (i) of this Table shows the input data. On the next page, Panel (ii) depicts the reconstructed data. The Padé-reconstructed data are converged at $N/16 = 64$, where $N = 1024$. In parentheses, immediately above each of these latter converged parameters are the related spectral parameters obtained at $N/32 = 32$. When the peaks have not yet been identified at this latter signal length, the missing spectral parameters are denoted as (–). Adapted from Refs. [14,15]

Metabolite		Benign				Malignant			
k	Assignment	$\mathrm{Re}(f_k)$ (ppm)	$\mathrm{Im}(f_k)$ (ppm)	d_k (au)	Concentration (μmol/L)	$\mathrm{Re}(f_k)$ (ppm)	$\mathrm{Im}(f_k)$ (ppm)	d_k (au)	Concentration (μmol/L)
(i) Input data									
1	Isoleucine (Iso)	1.02	0.000832	0.003060	10	1.02	0.000832	0.024174	79
2	Valine (Val)	1.04	0.000831	0.034578	113	1.04	0.000831	0.120869	395
3	Threonine (Thr)	1.33	0.000830	0.027540	90	1.33	0.000830	0.075887	248
4	Lactate (Lac)	1.41	0.000829	0.758570	2479	1.41	0.000829	2.000000	6536
5	Alanine (Ala)	1.51	0.000828	0.089657	293	1.51	0.000828	0.179315	586
6	Lysine (Lys)	1.72	0.000827	0.030906	101	1.72	0.000827	0.149939	490
7	Methionine (Met)	2.13	0.000826	0.002142	7	2.13	0.000826	0.018972	62
8	Glutamine (Gln)	2.47	0.000825	0.084149	275	2.47	0.000825	0.253366	828
9	Creatine (Cr)	3.05	0.000824	0.019278	63	3.05	0.000824	0.020196	66
10	Creatinine (Crn)	3.13	0.000823	0.020808	68	3.13	0.000823	0.024174	79
11	Choline (Cho)	3.19	0.000822	0.004590	15	3.19	0.000822	0.012852	42
12	Glucose (Glc)	5.22	0.000821	0.424419	1387	5.22	0.000821	0.079559	260

Table 3 continued

Metabolite		Benign				Malignant			
k	Assignment	Re(f_k) (ppm)	Im(f_k) (ppm)	d_k (au)	Concentration (μmol/L)	Re(f_k) (ppm)	Im(f_k) (ppm)	d_k (au)	Concentration (μmol/L)
(ii) Reconstructed data									
1	Isoleucine	(–)	(–)	(–)	(–)	(–)	(–)	(–)	(–)
	(Iso)	1.02	0.000832	0.003060	10	1.02	0.000832	0.024174	79
2	Valine (Val)	(1.04)	(0.001126)	(0.038144)	(125)	(1.04)	(0.001385)	(0.148345)	(485)
		1.04	0.000831	0.034578	113	1.04	0.000831	0.120869	395
3	Threonine	(–)	(–)	(–)	(–)	(–)	(–)	(–)	(–)
	(Thr)	1.33	0.000830	0.027540	90	1.33	0.000830	0.075887	248
4	Lactate	(1.41)	(0.001112)	(0.796695)	(2604)	(1.41)	(0.001359)	(2.046777)	(6689)
	(Lac)	1.41	0.000829	0.758570	2479	1.41	0.000829	2.000000	6536
5	Alanine	(1.48)	(0.005242)	(0.081618)	(267)	(1.45)	(0.008354)	(0.196311)	(642)
	(Ala)	1.51	0.000828	0.089657	293	1.51	0.000828	0.179315	586
6	Lysine (Lys)	(1.71)	(0.009103)	(0.035289)	(115)	(1.71)	(0.004174)	(0.174566)	(571)
		1.72	0.000827	0.030906	101	1.72	0.000827	0.149939	490
7	Methionine	(2.21)	(0.216911)	(0.005434)	(18)	(2.10)	(0.031194)	(0.028735)	(94)
	(Met)	2.13	0.000826	0.002142	7	2.13	0.000826	0.018972	62
8	Glutamine	(2.47)	(0.000827)	(0.082597)	(270)	(2.47)	(0.000829)	(0.251929)	(823)
	(Gln)	2.47	0.000825	0.084149	275	2.47	0.000825	0.253366	828
9	Creatine	(3.06)	(0.001584)	(0.020058)	(66)	(3.07)	(0.003142)	(0.028426)	(93)
	(Cr)	3.05	0.000824	0.019278	63	3.05	0.000824	0.020196	66
10	Creatinine	(3.14)	(0.002581)	(0.024700)	(81)	(3.17)	(0.003443)	(0.028564)	(93)
	(Crn)	3.13	0.000823	0.020808	68	3.13	0.000823	0.024174	79
11	Choline	(–)	(–)	(–)	(–)	(–)	(–)	(–)	(–)
	(Cho)	3.19	0.000822	0.004590	15	3.19	0.000822	0.012852	42
12	Glucose	(5.22)	(0.000821)	(0.424418)	(1387)	(5.22)	(0.000821)	(0.079557)	(260)
	(Glc)	5.22	0.000821	0.424419	1387	5.22	0.000821	0.079559	260

of 1.02–1.04 ppm differ significantly in these two types of lesions [30]. The high concentrations of these branched chain amino acids are seen as protein breakdown products due to necrosis and proteolysis. When the customary (non-optimal) data analytical methods are used, the so-named "spectral crowding" has been noted to be a major problem in delineating these closely-lying resonances.

The presented results from Refs. [14,15] strongly suggest that the high resolution of the fast Padé transform could help improve SNR, which has been a major obstacle to the progress of in vivo applications of MRS for ovarian cancer diagnostics. Most importantly, without any fitting or numerical integration of peak areas (the latter was used in Ref. [30]), the FPT reliably yields the metabolite concentrations of primary significance for distinguishing benign from malignant ovarian lesions. These features of the FPT are deemed to be of critical benefit to ovarian cancer diagnostics via magnetic resonance spectroscopy, in particular for early detection, a goal which has thus far been elusive, but achievement of which would definitely confer a major survival advantage.

4 Importance of the results for research and clinical oncology

The results presented in this work are demonstrated to be of clear, direct and immediate importance for clinical oncology. Since MRS and MRSI are increasingly recognized as one of the key modalities for cancer diagnostics, surmounting the shortcomings of current applications of these two modalities represents an urgent priority. Padé-optimization offers a distinct possibility to realize this goal.

Besides confirming the high resolution and stability of the FPT in general studies of MR total shape spectra [1–4], and thereby overcoming one of the major hindrances to wider application of MRS and MRSI in oncology, we have now shown this superior resolution performance with respect to data directly derived from malignant and benign ovarian samples [14,15]. This is the first time that the FPT has been applied to this problem area. From the clinical viewpoint, it is important to mention that the small size and motion of this organ have created major problems for in vivo applications of MRS. Thus far, there have been only a few investigations applying in vivo MRS to evaluate cancerous ovarian lesions [31–34]. Altogether, some 18 malignant and 54 benign lesions of various histopathology, as well as one borderline cancerous adnexal mass have been examined in this way. Only a limited number of metabolites could be identified and evaluated and their concentrations were estimated qualitatively with inconclusive results. It has been suggested that insofar as the current problems hindering encoding of high quality time signals are overcome, in vivo ^{1}H MRS could become the method of choice for evaluating ovarian lesions [35]. The present results strongly suggest that Padé-optimized MRS could be instrumental here, as well.

In the present work, we have described our studies by establishing that the FPT provides exact quantification of brain MRS time signals that closely match FIDs encoded in vivo by clinical scanners at 1.5 T [5,9,12,25]. The highly precise concentrations (to 12 digits of accuracy) are given for 25 metabolites, including those which are closely lying and even those which almost completely overlap. Likewise, we have proven [14,15] that the FPT is capable of exactly reconstructing all the six digit accurate input spectral parameters of 12 metabolites for benign and malignant

ovarian cyst fluid MRS time signals that are derived from in vitro FIDs encoded with a high-resolution 600 MHz NMR spectrometer [30], or equivalently, $B_0 = 14.1$ T. Such machine accuracy in simple [14,15] or double precision [5,6] is sought to benchmark the FPT on the fully controlled input FID. *Passing this most stringent test is far from being academic.* Quite the contrary, those estimators that cannot achieve a comparable accuracy as the FPT for fully controlled FIDs have no chance whatsoever for reliable performance in the case of uncontrolled FIDs such as those encoded in vivo by means of MRS. Indeed, the maximal sought accuracy which is possible for noise-corrupted synthesized or encoded FIDs is 3–4 stable digits in the reconstructed concentrations of the genuine, clinically relevant metabolites. This level of the requested accuracy has been demonstrated to be readily achievable by the FPT for both synthesized noise-corrupted FIDs [6] and encoded, in vivo time signals [9–11]. It should be emphasized that the majority of in vivo MRS studies have been based upon estimates of at most four or five, or often even fewer metabolites [26]. As discussed in [13], in vivo MRS studies of the breast cancer have been mainly based only upon estimates of total choline. On the other hand, in vitro MRS findings for a wide array of human cancers clearly distinguish malignant and normal tissues, and frequently offer insights into molecular mechanisms. The most important information for detecting malignant lesions is often found in closely overlapping resonances, some of which decay rapidly and therefore can only be detected at short acquisition times, as well as those in low concentration [26,27]. The present studies [5,9,12,25] show that the FPT offers greater possibilities to extract this rich spectroscopic information, which heretofore has remained untapped with the conventional Fourier approach. Therefore, these studies can be considered as *benchmark* and a *paradigm shift*. Together with the practical implementation described in [13], a valid, exact and highly practical approach to quantification of MRS signals has now been achieved by means of the FPT, and this could have profound implications for improving the accuracy with which malignancies are diagnosed via MRS.

Distinguishing genuine from spurious ("noisy" or "noise-like") information has been a major difficulty for MRS. All post-processing fitting algorithms are limited to guesswork about how many true metabolites actually underlie a given peak in the shape spectrum. Such a dilemma is a critical stumbling block for clinical oncology: many contradictory findings in tumour diagnostics are related to whether or not a given metabolite was included in the original expansion basis sets such as those used in e.g., the LCModel [36,37]. In our recent papers [6,25] via the powerful concept of Froissart doublets (pole-zero cancellation), the FPT has been shown to solve this problem fully. A succinct summary of how this is accomplished is provided in the present study for MR time signals corrupted with noise at the levels typically encountered in clinical scanners with good SNR. Thus, for the first time it is now possible to compute metabolite concentrations without guessing or ambiguity about the veracity of this information. This novel approach is benchmarked via the Froissart doublets within the FPT, and is given the name: "*Signal–Noise Separation*" as abbreviated accordingly by SNS. We emphasize once again that the number of spurious resonances is always several times greater than the true metabolites. In the present illustrations there were 128 resonances, but only 25 were genuine. Thus, 103 or over 80% were spurious. It is, therefore, clearly of utmost importance for trustworthy clinical applications that the genuine information be identified.

Early detection of ovarian cancer is an urgent priority because of the dramatic survival advantage this definitely would confer. When involving only the ovary itself (Stage Ia), 5-year survival rates for ovarian cancer are 90% or better. However, the vast majority of ovarian cancers are diagnosed after they have spread to the abdomen (Stage III or higher), such that overall 5-year survival rates are very poor (less than 20%) [38]. However, existing screening methods do not offer specificity for ovarian cancer in its early stages [39–41]. Our focus upon ovarian cancer should be seen within the context of the on-going intensive work to find better methods for early ovarian cancer detection. Not only does the FPT markedly enhance resolution of MR spectra, but it also yields the unequivocal, exact parametric data needed to reconstruct the metabolite concentrations which characterize ovarian cancer and distinguish this from non-malignant samples.

We have begun investigations along these lines for breast and prostate cancer as well as melanoma using the FPT; preliminary results are described in [13]. Therein we also describe preliminary findings applying the FPT to MRI, 2D MRS and to MRSI, with attention to improved target definition for radiotherapy.

A number of our recent publications have been directly and explicitly concerned with the relevance of Padé-based molecular imaging through magnetic resonance for clinical oncology [4,7,14,15,26,42–48]. We have paid particular attention to the shortcomings of current applications of MR-based modalities for cancer diagnostics and their relationship to reliance upon the conventional Fourier method of data analysis. We have shown that dilemmas surrounding metabolite assignment, the non-uniqueness of fitting and quantification, as well as poor resolution and unfavorable SNR, represent major obstacles for clinical MRS and MRSI with respect to timely tumor identification, histological classification, tumor grading, assessment of response to therapy and early detection of tumor recurrence. Our work specifically related to brain tumor diagnostics includes Refs. [26,44]. Also, Padé-based MRS and MRSI has been applied in the context of early detection of cancers, especially ovarian [14,15], prostate [26] and breast cancer [45–48]. We have performed detailed paired and logistic regression analysis [45–47] which confirmed that a very rich "window" of information is provided by in vitro ^{1}H MRS analysis of metabolite concentrations in malignant versus non-cancerous breast tissue. This rich source of information could be tapped with Padé-based signal processing of MRS and MRSI signals encoded from the breast.

We anticipate that MRS via Padé processing will reduce the false positive rates of MR-based modalities and, moreover, will further improve the sensitivity of these methods. Once this is achieved, and given that all MR-based diagnostic methods are free from ionizing radiation, new possibilities for cancer screening and early detection will open up, especially for risk groups, e.g., the application of Padé-optimized MRS in younger women at high risk for breast and/or ovarian cancer. The need for accurate quantification of closely overlapping resonances has been particularly underscored for breast cancer diagnostics using MRS. Further, MRS with the accompanying Padé quantification applied to prostate cancer is particularly important for diagnostic enhancement, because of the current dilemmas surrounding prostate cancer screening [e.g., cutpoints of prostate specific antigen (PSA), etc], as well as the public health importance of this malignancy. Also, there is a great need for non-invasive diagnostic support for physicians in the early detection of malignant melanomas. A person may

have up to 100 moles, and to distinguish between malignant melanomas and benign nevi is very difficult even for an experienced dermatologist. For a general practitioner, it is often an impossible task. Padé-optimized MRS seems to be an excellent candidate for further studies in this field by providing quantitative standards to better differentiate malignant melanomas from benign lesions.

The strategic importance for clinical oncology of robust and uniform data processing of MRS signals has been strongly emphasized by leading experts internationally, including the U.S. National Cancer Institute. Particular emphasis has been placed on the need for reliable quantitative information in cancer diagnostics with respect to MRS [26,27,35,49–53].

On the basis of our work thus far, it follows that the fast Padé transform fulfills the most stringent conditions for tumor diagnostics within magnetic resonance due to the following critical features of this versatile estimator:

(i) Markedly enhanced resolution and signal-to-noise ratio compared to the conventional Fourier-based techniques,
(ii) Provides precise numerical data for all peak parameters (position, height, width and phase) for every true metabolite,
(iii) Specifies the exact number of metabolites from the encoded time signals and can identify unambiguously overlapping metabolites, as well as metabolites present in low concentrations, both of which are very often of critical clinical importance,
(iv) Obtains the amplitude of each metabolite most accurately and separately from an analytical expression dependent only upon the metabolite's frequency, thus obviating the customary need for solving a system of linear equations,
(v) By the Froissart filter efficiently separates noise from genuine metabolic information,
(vi) Undergoes rigorous validation and error analysis,
(vii) Yields itself to efficient programming with optimally accurate results, and
(viii) Extends directly, in a straight-forward manner to multidimensional signal and image processing, with cross-dimensional coherence, thus bypassing the sequential one-dimensional approach of Fourier analysis.

Overall, we can say that this line of endeavor lays the basis for the next phase of research activity in which the major goal is to further improve the resolution and diagnostic accuracy of MR-based methods, and for Padé-based MRS and MRSI to become standard tools for clinical oncology.

5 Conclusion

Traditionally, the Padé approximant for any given power series is defined by the unique quotient of two polynomials. However, the fast Padé transform, denoted by FPT, does not necessarily require a power series as the usual starting point. For example, the FPT is naturally ingrained in the Schrödinger picture of quantum mechanics and in the total time-independent Green function for the studied system. The FPT is an efficient solver of generalized eigenvalue problems, such as the quantum-mechanical evolution/relaxation matrix comprised of auto-correlation functions. These generic functions can be

either obtained theoretically or measured experimentally. Auto-correlation functions represent a veritable alternative formulation of quantum mechanics.

We demonstrate the advantages of the FPT relative to the fast Fourier transform, the FFT, which is a single polynomial. Namely, the FPT can analytically continue general functions outside their initial convergence domains and can evaluate the spectrum at any energy or frequency, whereas the FFT has no interpolation/extrapolation features due to its restriction to the fixed Fourier grid points. Unlike the FFT which supplies only the shape of a spectrum, the parametric FPT provides the exact number of spectral components, including those which overlap, and precise quantification of all four parameters (position, width, height, phase). Resolution in the FFT is low and limited by its linearity. By contrast, the FPT is a non-linear estimator with a high resolving power beyond the Rayleigh-Fourier bound which is constrained by the total acquisition time. Moreover, unlike nearly all other parametric estimators which show wild oscillations, the FPT exhibits a remarkably stable convergence with increasing signal length. Finally, among all other signal processors, the FPT has the unique capability to unequivocally separate the physical from nonphysical content of time signals embedded in noise. The ensuing capacity of the FPT for signal–noise separation, the SNS, is reliably accomplished by the Froissart filter.

The Froissart filter for identification of spurious resonances is based upon the appearance of Froissart doublets that enable cancellation of nonphysical poles and zeros in the rational response function of generic systems exposed to external perturbations. Hence the term "pole-zero cancellations." A spurious resonance in a spectrum appears as a nonphysical peak with its complex frequencies and amplitudes. Genuine peaks are also fully characterized by complex frequencies and amplitudes, so the problem is how to distinguish the true from the false information. The solution to this extremely difficult and challenging problem is provided by the FPT, because this method can identify with fidelity every false resonance by realization that all spurious pole are automatically accompanied by the corresponding spurious zeros. These spurious pole-zero pairs are called Froissart doublets, according to their discoverer who was the first to notice this remarkably important phenomenon in a numerical experiment. By contrast, physical poles and zeros do not coincide with each other. Such a clear distinction gives the possibility to unequivocally separate spurious from genuine resonances. Computationally, the FPT achieves this separation by rooting both the numerator and denominator polynomials. Since the Padé quotient is a meromorphic function, the zeros of the numerator and denominator polynomial are the zeros and poles of the response function, which is the frequency spectrum given by the unique polynomial quotient. From the set of all the reconstructed poles and zeros, the spurious couples are identified as Froissart doublets whenever the corresponding poles and zeros coincide with each other. Once identified in this way, all the spurious resonances can be discarded, and this constitutes the Froissart filter. Therefore, by means of the Froissart filter, all the remaining spectral features are exclusively genuine, physical resonances. In the present study we show that the resulting SNS concept can even visually be spotted via the Argand plot for all the retrieved complex frequencies. In such a two-dimensional plot, showing the imaginary versus real frequencies, the confluence of spurious poles and zeros is at once noticed by the emergence of the Froissart doublets only for the negative values of imaginary frequencies. These latter

frequencies are unphysical, since they cause the complex harmonics in the time signal to increase exponentially, thus leading to divergence. In sharp contrast, all the genuine frequencies appear in the Argand plot with positive imaginary frequencies for which the complex harmonics contain only decreasing exponentials with the ensuing convergence of signal as the time becomes infinitely large. In other words, in the Argand plot, there is a sharp and strict visual separation between the genuine and spurious frequencies, because they reside in two disjoint parts of the complex frequency plane. The accompanying confirmation of the identification of all the Froissart frequencies is another extraordinary occurrence, which consists of yielding zero values of the spurious amplitudes. This is physically plausible, and it also becomes immediately obvious from the Cauchy residue formula for the amplitudes in the polynomial canonical form which is annulled automatically, whenever poles and zeros of the response function coincide. This is precisely the case, by definition, with the Froissart spurious resonances. In this way, the FPT offers a unique prescription for identifying nonphysical information from time signals by detecting the coincidence of spurious poles and zeros, as well as by identifying the zero values for the spurious amplitudes. One does not even need to bother to discard the found nonphysical resonances, because the spurious poles and zeros automatically cancel each other in the response function written in the canonical form of the polynomial quotient in the FPT. The equivalent of this pole-zero cancellation also takes place through zero-valued spurious amplitudes in the alternative representation of the response function given by the Heaviside partial fraction decomposition.

In the present illustrations, aside from being universally applicable to all time signals, we show how the SNS concept can become an invaluable tool to aid magnetic resonance spectroscopy, MRS, which is used as one of the most powerful modern modalities in early cancer diagnostics.

Acknowledgements This work has been supported by King Gustav the 5th Jubilee Foundation, the Karolinska Institute Research Fund and the Signe and Olof Wallenius Stiftelse.

References

1. Dž. Belkić, Strikingly stable convergence of the fast Padé transform (FPT) for high-resolution parametric and non-parametric signal processing of Lorentzian and non-Lorentzian spectra. Nucl. Instrum. Methods Phys. Res. A **525**, 366 (2004)
2. Dž. Belkić, Error analysis through residual frequency spectra in the fast Padé transform (FPT). Nucl. Instrum. Methods Phys. Res. A **525**, 379 (2004)
3. Dž. Belkić, Analytical continuation by numerical means in spectral analysis using the fast Padé transform (FPT). Nucl. Instrum. Methods Phys. Res. A **525**, 372 (2004)
4. Dž. Belkić, K. Belkić, The fast Padé transform in magnetic resonance spectroscopy for potential improvements in early cancer diagnostics. Phys. Med. Biol. **50**, 4385 (2005)
5. Dž. Belkić, Exact quantification of time signals in Padé-based magnetic resonance spectroscopy. Phys. Med. Biol. **51**, 2633 (2006)
6. Dž. Belkić, Exponential convergence rate (the spectral convergence) of the fast Padé transform for exact quantification in magnetic resonance spectroscopy. Phys. Med. Biol. **51**, 6483 (2006)
7. Dž. Belkić, K. Belkić, Decisive role of mathematical methods in early cancer diagnostics. J. Math. Chem. **42**, 1 (2007)
8. Dž. Belkić, Fast Padé transform for exact quantification of time signals in magnetic resonance spectroscopy. Adv. Quant. Chem. **51**, 157 (2006)

9. Dž. Belkić, K. Belkić, Fast Padé transform for optimal quantification of time signals from magnetic resonance spectroscopy. Int. J. Quantum. Chem. **105**, 493 (2005)
10. Dž. Belkić, Padé-based magnetic resonance spectroscopy (MRS). J. Comp. Meth. Sci. Eng. **3**, 563 (2003)
11. Dž. Belkić, K. Belkić, In vivo magnetic resonance spectroscopy by the fast Padé transform. Phys. Med. Biol. **51**, 1049 (2006)
12. Dž. Belkić, *Quantum Mechanical Signal Processing and Spectral Analysis* (Institute of Physics Publishing, Bristol, UK, 2004)
13. Dž. Belkić, K. Belkić, The general concept of signal–noise separation (SNS): mathematical aspects and implementation in magnetic resonance spectroscopy. J. Math. Chem. doi: 10.1007/s10910-007-9344-5
14. Dž. Belkić, K. Belkić, Mathematical modeling of an NMR chemistry problem in ovarian cancer diagnostics. J. Math. Chem. **43**, 395 (2007)
15. K. Belkić, Resolution performance of the fast Padé transform: Potential advantages for magnetic resonance spectroscopy in ovarian cancer diagnostics. Nucl. Instrum. Methods Phys. Res. A **580**, 874 (2007)
16. D.S. Stephenson, Linear prediction and maximum entropy methods in NMR spectroscopy. Prog. NMR Spectrosc. **20**, 515 (1988)
17. W.W.F. Pijnappel, A. van den Boogaart, R. de Beer, D. van Ormondt, SVD-based quantification of magnetic resonance signals. J. Magn. Reson. **97**, 122 (1992)
18. J.W.C. van der Veen, R. de Beer, P.R. Luyten, D. van Ormondt, Accurate quantification of in vivo 31P NMR signals using the variable projection method and prior knowledge. Magn. Reson. Med. **6**, 92 (1988)
19. L. Vanhamme, A. van den Boogaart, S. van Haffel, Improved method for accurate and efficient quantification of MRS data with use of prior knowledge. J. Magn. Reson. **29**, 35 (1997)
20. S.W. Provencher, Estimation of metabolite concentrations from localized in vivo proton NMR spectra. Magn. Reson. Med. **30**, 672 (1993)
21. M.R. Wall, D. Neuhauser, Extraction, through filter-diagonalization, of general quantum eigenvalues or classical normal mode frequencies from a small number of residues or a short time segment of a signal. I. Theory and application to a quantum-dynamics model. J. Chem. Phys. **102**, 8011 (1995)
22. V.A. Mandelshtam, FDM: the filter diagonalization method for data processing in NMR experiments. Progr. Nucl. Magn. Reson. Spectrosc. **38**, 159 (2001)
23. J. Frahm, H. Bruhn, M.L. Gyngell, K.D. Merboldt, W. Hanicke, R. Sauter, Localized high-resolution proton NMR spectroscopy using stimulated echoes: initial applications to human brain in vivo. Magn. Reson. Med. **9**, 79 (1989)
24. I. Tkáč, P. Andersen, G. Adriany, H. Merkle, K. Ugurbil, R. Gruetter, In vivo ^{1}H NMR spectroscopy of the human brain at 7T. Magn. Reson. Med. **46**, 451 (2001)
25. Dž. Belkić, Machine accurate quantification in magnetic resonance spectroscopy. Nucl. Instrum. Methods Phys. Res. A **580**, 1034 (2007)
26. K. Belkić, *Molecular Imaging through Magnetic Resonance for Clinical Oncology* (Cambridge International Science Publishing, Cambridge, UK, 2004)
27. P.A. Bottomley, The trouble with spectroscopy papers. J. Magn. Reson. Imaging **2**, 1 (1992)
28. M. Froissart, Approximation de Padé: Application à la Physique des Particules Élémentaires, CNRS, RCP, Programme No. 25. Strasbourg **9**, 1 (1969)
29. Dž. Belkić, P.A. Dando, J. Main, H.S. Taylor, Three novel high-resolution nonlinear methods for fast signal processing. J. Chem. Phys. **113**, 6542 (2000)
30. E. Boss, S.H. Moolenaar, L.F.A.G. Massuger, H. Boonstra, U.F.H. Engelke, J.G.N. de Jong, R.A. Wevers, High-resolution proton nuclear magnetic resonance spectroscopy of ovarian cyst fluid. NMR Biomed. **13**, 297 (2000)
31. S.W. Cho, S.G. Cho, J.H. Lee, H.-J. Kim, M.H. Lim, J.H. Kim, C.H. Suh, In-vivo proton magnetic resonance spectroscopy in adnexal lesions. Korean J. Radiol. **3**, 105 (2002)
32. S. Hascalik, O. Celik, G. Erdem, Magnetic resonance spectral analysis of ovarian teratomas. Int. J. Gynecol. Obstet. **90**, 152 (2005)
33. S. Hascalik, O. Celik, K. Sarak, M.M. Meydanli, A. Alkan, B. Mizrak, Metabolic changes in pelvic lesions: findings at proton MR spectroscopic imaging. Gynecol. Obstet. Invest. **60**, 121 (2005)
34. T. Okada, M. Harada, K. Matsuzaki, H. Nishitani, T.J. Aono, Evaluation of female intrapelvic tumors by clinical proton MR spectroscopy. Magn. Reson. Imaging **13**, 912 (2001)

35. L.F.A.G. Massuger, P.B.J. van Vierzen, U. Engelke, A. Heerschap, 1H-MR spectroscopy. A new technique to discriminate benign from malignant ovarian tumors. Cancer **82**, 1726 (1998)
36. K.S. Opstad, S.W. Provencher, B.A. Bell, J.R. Griffiths, F.A. Howe, Detection of elevated glutathione in meningiomas by quantitative in vivo 1H MRS. Magn. Reson. Med. **49**, 632 (2003)
37. Y.-D. Cho, G.-H. Choi, S.-P. Lee, J.-K. Kim, ^{1}H-MRS metabolic patterns for distinguishing between meningiomas and other brain tumors. Magn. Reson. Imaging **21**, 663 (2003)
38. S. Bhoola, W.J. Hoskins, Diagnosis and management of epithelial ovarian cancer. Obstet. Gynecol. **107**, 1399 (2006)
39. U.S. Preventive Services Task Force, Screening for ovarian cancer: recommendation statement. Ann. Fam. Med. **2**, 260 (2004)
40. N. Einhorn, R. Bast, R. Knapp, B. Nilsson, V. Zurawski, K. Sjövall, Long-term follow-up of the Stockholm screening study on ovarian cancer. Gynecol. Oncol. **79**, 466 (2000)
41. L. Cohen, Should transvaginal ultrasound be performed at annual examination in asymptomatic women? Int. J. Fertil. **48**, 150 (2003)
42. K. Belkić, Magnetic resonance spectroscopy and spectroscopic imaging: review of basic principles and achievements in oncology. J. Comp. Meth. Sci. Eng. **3**, 505 (2003)
43. K. Belkić, The need for quantitative biomedical spectroscopic imaging through magnetic resonance in oncology beyond the conventional Fourier-based framework for data analysis. J. Comp. Meth. Sci. Eng. **3**, 535–561 (2003)
44. K. Belkić, Dž. Belkić, Spectroscopic imaging through magnetic resonance for brain tumour diagnostics: recent achievements, dilemmas and potential solutions via advances in signal processing. J. Comp. Meth. Sci. Eng. **4**, 157 (2004)
45. K. Belkić, Magnetic resonance spectroscopic imaging in breast cancer detection: possibilities beyond the conventional theoretical framework for data analysis. Nucl. Instrum. Methods Phys. Res. A **525**, 313 (2004)
46. Dž. Belkić, K. Belkić, Mathematical optimization of in vivo NMR chemistry through the fast Padé transform: potential relevance for early breast cancer detection by magnetic resonance spectroscopy. J. Math. Chem. **40**, 85 (2006)
47. K. Belkić, Current dilemmas and future perspectives for breast cancer screening with a focus upon optimization of MR spectroscopic imaging by advances in signal processing. Isr. Med. Assoc. J. **6**, 610 (2004)
48. K. Belkić, Padé-optimized magnetic resonance spectroscopy: New possibilities for early breast cancer detection. Medicinteknikdagarna, October 2006, Uppsala
49. J. Evelhoch, M. Garwood, D. Vigneron, M. Knopp, D. Sullivan, A. Menkens, et al., Expanding the use of magnetic resonance in the assessment of tumor response to therapy. Cancer Res. **65**, 7041 (2005)
50. A. Maudsley, Can MR spectroscopy ever be simple and effective? Am. J. Neuroradiol. **69**, 2167 (2005)
51. R. Katz-Brull, P.T. Lavin, R.E. Lenkinski, Clinical utility of proton MR spectroscopy in characterizing breast lesions. J. Natl. Cancer Inst. **94**, 1197 (2002)
52. E. Danielsen, B. Ross, *Magnetic Resonance Spectroscopy Diagnosis of Neurological Diseases* (Marcel Dekker, Inc, New York, USA, 1999)
53. Brandão, R. Domingues, *MR Spectroscopy of the Brain* (Lippincott Williams & Wilkins, Philadelphia, USA, 2004)